RSC Advances

ROYAL SOCIETY OF CHEMISTRY

www.rsc.org/advances

Cite this: DOI: 10.1039/c0xx00000x

www.rsc.org/xxxxxx

ARTICLE TYPE

Controlled Synthesis of Pyrochlore $Pr_2Sn_2O_7$ Nanospheres with Enhanced Gas Sensing Performance†

Qi Liu,*[a] Miao Xu,[a] Ze-Xian Low,[c] Wen Zhang,[a] Feng Tao,[a] Feng Liu,[b] Ning Liu[a]

Received (in XXX, XXX) Xth XXXXXXXXX 20XX, Accepted Xth XXXXXXXXX 20XX

DOI: 10.1039/b000000x

Uniform $Pr_2Sn_2O_7$ nanospheres were synthesized via a simple solvothermal route with ethylenediamine as the solvent. The as-prepared $Pr_2Sn_2O_7$ nanospheres with the diameters of 20–50 nm are composed of nanoparticles with a size of 3–5 nm. The introduction of water into the reaction solution results in the formation of smaller $Pr_2Sn_2O_7$ nanospheres with poor crystallinity or SnO_2 particles indicating that ethylenediamine plays complicated effects on the generation of $Pr_2Sn_2O_7$ nanospheres. The UV-vis spectrum reveals that the band-gap of synthesized $Pr_2Sn_2O_7$ nanospheres is about 4.19 eV, much higher than the theoretical calculation value by DFT. The enhanced gas sensing performances could be attributed to the unique mesoporous nanospheres structure, which can significantly facilitate gas diffusion and mass transportation in sensing materials.

Introduction

The physical and chemical performance of materials are determined not only by their chemical composition, but also by their physical dimensions, structures, shapes and sizes.[1-3] In recent decades, considerable progress has been made in size- and shape-controlled synthesis of nanocrystals. Nanoporous spheres have attracted a great deal of attention because of their unique structural, physical and chemical properties such as high specific surface area, low density, and good permeation.[4-7] Hence, the fabrication of nanospheres with pores sizes ranging from one to hundreds of nanometersis critically important for both scientific research and technological development.

Due to their catalytic activity, defect structures, unique mechanical properties and high thermal stability,[8-11] lanthanide stannate pyrochlores $Ln_2Sn_2O_7$ (Ln = lanthanide elements) with cubic pyrochlore structure (Fd3m) have emerged as prospective materials for different applications such as catalysts, dielectrics, fast ion conductors, superconductors, ferromagnets and hosts for radioactive waste.[8-11]The conventional method for the preparation of $Ln_2Sn_2O_7$ is a solid-state reaction by calcining tin oxide with lanthanide oxide at high temperature(about 1500°C) for a long time (up to 5 d).[12-16] The obtained powders usually show extensive aggregation and compositional inhomogeneity, which degrades their performance. Recently, much emphasis has been paid on developing low-temperature liquid phase methods to get nanosize pyrochlore structures with shape and size control.[17-19] However, Sn^{4+}ions are easily hydrolyzed and there are distinct differences between Sn^{4+} and Ln^{3+} of physicochemical properties. It is difficult to prepare Sn-based pyrochlores via wet chemical approaches. Only few $Ln_2Sn_2O_7$ nanocrystals have been successfully synthesized via facile hydrothermal methods with good performance such as high photocatalytic activity,[18,19] ionically conducting properties at high temperatures.[17]

Among the lanthanide stannates, $Pr_2Sn_2O_7$ was reported as a new dynamic spin ice.[15,16] Due to the large ionic radius and small moment of Pr^{3+}, pyrochlore oxide $Pr_2Sn_2O_7$ is the most promising candidates for observation of strong quantum effects.[13] The conventional preparation method of $Pr_2Sn_2O_7$ is a solid-state reaction.[13,15,16] To the best of our knowledge, there is no report on the preparation of $Pr_2Sn_2O_7$ pyrochlore nanocrystals by wet chemical approaches and their application in gas-sensing. In this study, stoichiometric $Pr_2Sn_2O_7$ nanospheres were prepared by a facile solvothermal method with ethylenediamine (en) as the solvent. The synthesized $Pr_2Sn_2O_7$ nanospheres (ca. 20–50 nm) consist of nanoparticles with a size of 3–5 nm. To demonstrate the potential applications, the gas-sensing properties of $Pr_2Sn_2O_7$ nanospheres were investigated. A comparative gas sensing study between the as-synthesized $Pr_2Sn_2O_7$ nanospheres and SSR-$Pr_2Sn_2O_7$ was performed to demonstrate the enhanced gas sensing properties of the 3D porous $Pr_2Sn_2O_7$ materials.

Experimental

Preparation of the$Pr_2Sn_2O_7$ particles

All the chemicals were of analytical grade and used as received without further purification. The $Pr_2Sn_2O_7$ nanospheres were synthesized by a simple solvothermal route with en as the solvent. In a typical synthesis, 0.318 g of $Pr(CH_3COO)_3$ (1 mmol) and

[a] *Department of materials science and Engineering, Anhui Polytechnic University, Wuhu, Anhui241000, P. R. China.*
Fax: +86553 2871 252 ; Tel: +86 553 2871 252
E-mail: modieer_67@ahpu.edu.cn
[b]*College of Mathematics and Physics, Anhui Polytechnic University, Wuhu 241000, P. R. China.*
[c]*Department of Chemical Engineering, University of Bath, Claverton Down, Bath BA2 7AY, United Kingdom*
†Electronic Supplementary Information (ESI) available: characterizations and supporting images. See *DOI: 10.1039/b000000x*

0.351g of $SnCl_4 \cdot 5H_2O$ (1 mmol) were added to 15 mL en. The mixture was stirred for 40 min and then transferred to a stainless steel, Teflon-lined autoclave of 25 mL inner volume. Solvothermal synthesis was performed under an auto-generated pressure at 180 ℃ for 24 h in an electric oven, followed by natural cooling to room temperature. The product was collected by centrifugation, washed thoroughly with deionized water and ethanol for 3 times, respectively, and then dried at 80 °C for 12 h.

Characterization

The crystallographic phase of these as-prepared products was determined by an X-ray diffractometer (XRD) (Rigaku Ultima III, Japan) using Cu Kα radiation (λ= 0.154178 nm) at 40 kV and 40 mA. The XRD patterns were obtained over the scanning range of 10°–80° at room temperature with a scan rate of 10° min^{-1}. The morphology of the powders was examined by field emission scanning electron microscopy (FESEM, FEI NOVA NANOSEM 230). Transmission electron microscopy (TEM) and high-resolution transmission electron microscopy (HRTEM) images were obtained on a JEOL JEM–2100 microscope with a LaB_6 filament and an accelerating voltage of 200 kV. The UV–vis diffuse reflectance spectrum was recorded with a UV–vis spectrophotometer (UV–2550, Shimadzu) at room temperature and transformed to the absorption spectrum according to Kubelka–Munk relationship. The specific surface area of the samples was measured by nitrogen sorption at 77 K on a surface area and porosity analyzer (Micromeritics TriStar 3000, USA) and calculated by the BET method.

Gas-sensing test

$Pr_2Sn_2O_7$ samples were mixed with deionized water to form pastes. The pastes were coated onto the surface of an Al_2O_3 microtube with four Pt electrodes. The coating process was repeated several times to obtain the desired coating. Then the coated Al_2O_3 microtube was welded on a pedestal with six poles. And a heating coil was inserted through the Al_2O_3 microtube and its two ends were welded to the other two poles of the pedestal. The ethanol sensing characteristics of the prepared sensors were measured using a JF02E gas sensor test system (Kunming Guiyan Jinfeng technology Co. Ltd). Different concentrations of ethanol vapors (100–600 ppm) were used as the target gas to test the sensing performance of the samples. The time taken by the sensor to achieve 90% of the total resistance change was defined as the response time in the case of adsorption and the recovery time in the case of desorption.

Results and discussion

Typical XRD pattern of the as-prepared sample with reaction times of 24 h is shown in Fig. 1(a). All of the X-ray diffraction peaks are indexed to the cublic pyrochlore-type $Pr_2Sn_2O_7$ (JCPDS13-0184) with the lattice constant a = 1.0604 nm, which is in good agreement with the standard card. No impurity peaks such as those of SnO_2 or $Pr(OH)_3$ were detected, indicating the phase-pure $Pr_2Sn_2O_7$ of the product. This result indicates that the crystalline $Pr_2Sn_2O_7$ can be formed using the aforementioned facile solvothermal method at a relatively low temperature. The crystal structure of $Pr_2Sn_2O_7$ material is also shown in Fig.1b and Fig.1c. The crystalline has the cubic pyrochlore structure with space group *Fd*3*m* and contain eight formula units per unit cell. The Pr ions (III) are surrounded by eight oxygen atoms in a distorted cubic polyhedron, with the Sn IV ions coordinated by six oxygen atoms in an octahedron configuration.

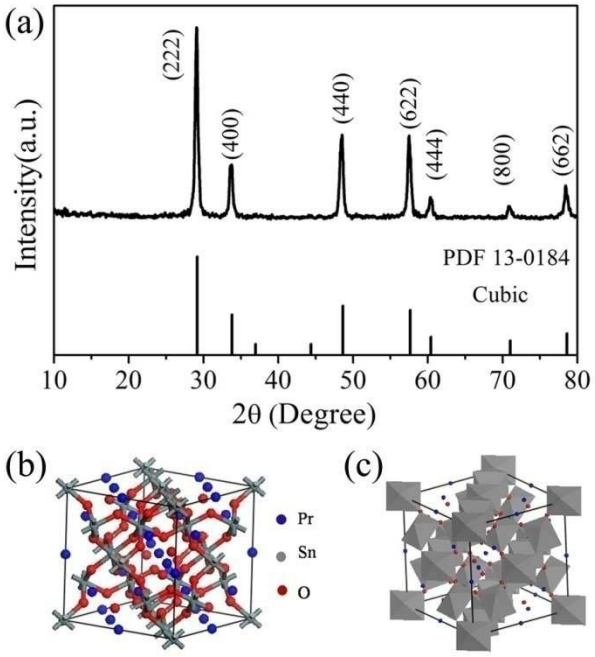

Fig.1 (a) XRD pattern of the $Pr_2Sn_2O_7$ crystalline, and cubic pyrochlore crystal structure of the$Pr_2Sn_2O_7$ crystalline: (b) the ball-and-stick model, (c) the polyhedron model.

Morphologies of the samples were examined by FE-SEM at room temperature, as shown in Fig.2. The lower magnification of the FE-SEM images in Fig.2a clearly show that a typical sample has a hierarchical structure of colloidal spheres with a diameters between 20–50 nm. These spheres were formed from numerous primary nanoparticles, as seen on the rough surface of the sample. It was also observed that the particle packing was not close-packed but was randomly agglomerated. The size of the primary nanoparticles was too small to conclusively determine the diameter from the SEM images. Energy dispersive spectrum(EDS) analysis indicates that the molar ratio of Pr:Sn is about 1:1, close to the $Pr_2Sn_2O_7$ stoichiometirc composition (Fig.S1). Transmission electron microscopy (TEM) images further demonstrate the high uniform pellet-like aggregates with a diameters of 20–50 nm, which consist of uniform tiny nanoparticles with a size of several nanometers (Fig. S2 and Fig.2c). More details can be found in the inset of Fig.2(c), which demonstrate that each pellet-like aggregate is composed of abundant randomly assembled nanoparticles with the size of 3–5 nm. Besides, the obvious contrast between the dark parts and the relatively bright parts in this TEM image reveals that the sphere is porous, which endows the $Pr_2Sn_2O_7$ with high surface area. The typical enlarged lattice-resolved HRTEM image of a nanoparticle (Fig. 2d) shows the clear crystal lattice fringes and the interplane distances are about 2.65Å, which matches well with the (400) planes of cublic pyrochlore-type $Pr_2Sn_2O_7$. The bright rings in the selected-area electron diffraction (SAED) pattern of a pellet-like aggregate (the inset of Fig.2d) can be well indexed to diffraction

from the (222), (400), (440) and (444) planes of cubic pyrochlore-type $Pr_2Sn_2O_7$, which indicates the polycrystalline characteristic assembling nature of nanoparticles.

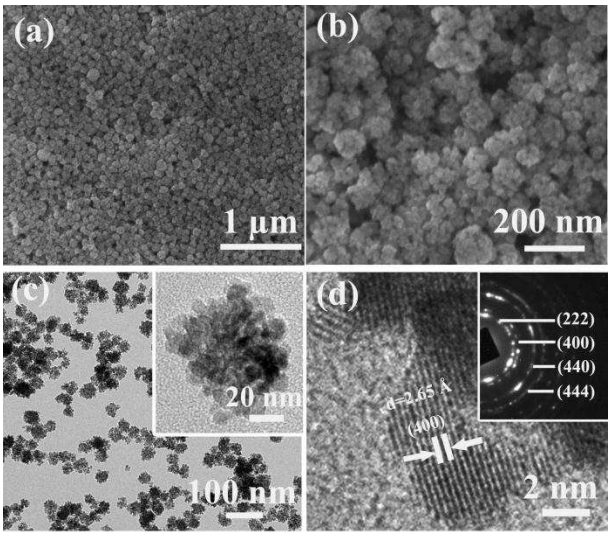

Fig.2 (a, b) FE-SEM, (c) TEM, and (d) HRTEM images of the $Pr_2Sn_2O_7$ crystalline. The inset of (c) shows the TEM image and inset of (d) shows SAED pattern obtained from a nanosphere.

Time-dependent evolution of morphology of $Pr_2Sn_2O_7$ nanospheres were studied by FE-SEM. Fig.3 shows typical morphologies of the products obtained at different stages (1, 4, 8 h and 12 h, respectively) of solvothermal reaction at a synthesis temperature of 180 °C. Very small floccus were formed after 1 h of reaction(Fig.3a). When the reaction was prolonged to 4 h, nanoparticles with relatively spherical shape were appeared (Fig.3b). The diameter of the clusters was measured to be 10–60 nm. After a reaction time of 8 h, relatively uniform incompact colloidal spheres with rough surface became dominant (Fig.3c) and there are still some nanoparticles of several nanometers in size. When the reaction time was further prolonged to 12 h, the small $Pr_2Sn_2O_7$ nanoparticles almost disappeared and the $Pr_2Sn_2O_7$ nanospheres become more uniform in size and shape.

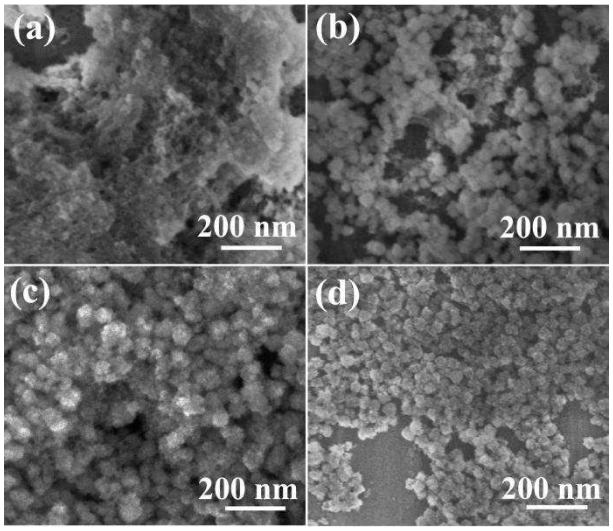

Fig.3 FE-SEM images of $Pr_2Sn_2O_7$ synthesized at different solvothermal reaction times:(a) 1h, (b) 4 h, (c)8 h,(d) 12 h

The phase and purity of the as-obtained samples with reaction times of 1 h, 4 h, 8 h and 12 h were also determined by XRD, and typical diffraction patterns are shown in Fig.4. No XRD peaks of $Pr_2Sn_2O_7$ appear after 1 h of reaction. There is a broad diffraction peak between 20–35° and a small diffraction peak at ~51°, which could be attributed to tetragonal phase SnO_2 (JCPDS, 41-1445) and the sample could be amorphous SnO_2. When the reaction was prolonged to 4 h, the diffraction peaks of $Pr_2Sn_2O_7$ phase are observed, together with some unreacted SnO_2. With further prolonged synthesis, the XRD peaks attributed to SnO_2 disappear while the XRD peaks of $Pr_2Sn_2O_7$ become prominent. The XRD patterns of the products prepared for 8, 12, and 24 h (see Fig. 1) seem to be almost the same, except for slightly increasing in XRD intensity with the reaction time being prolonged. When the reaction time was increased from 1 to 24 h, the diffraction peaks became narrower, consistent with the bigger particle sizes.

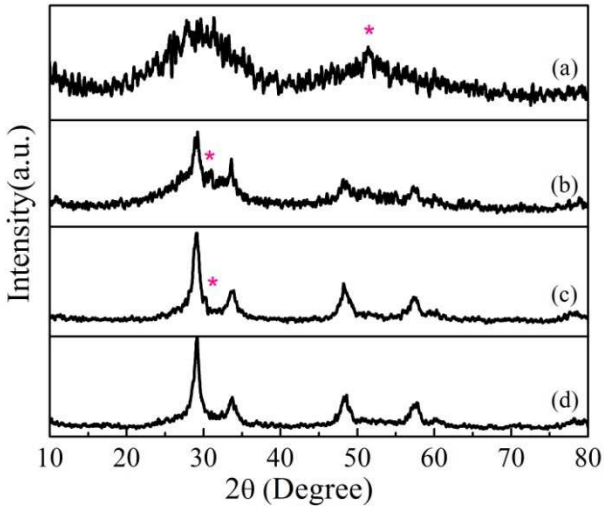

Fig.4 XRD patterns of $Pr_2Sn_2O_7$ synthesized at different solvothermal reaction times:(a) 1h, (b) 4 h, (c)8 h,(d) 12 h

Fig. 5. shows the UV-vis absorption spectrum of $Pr_2Sn_2O_7$ sample synthesized at different reaction times. A significant blue shift of the main absorption edge in the absorption spectra has

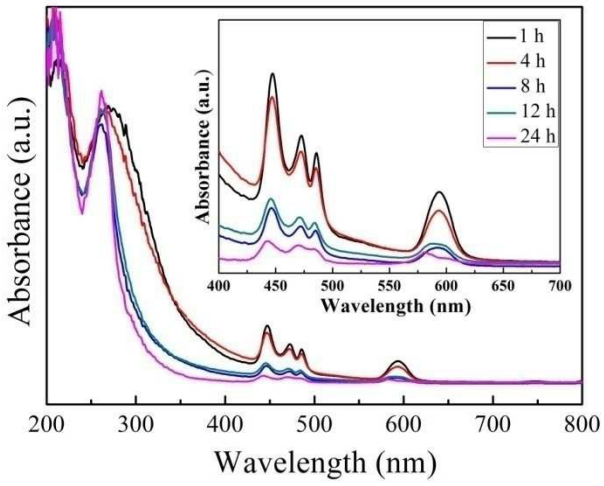

Fig.5 UV-vis absorption spectrum of the $Pr_2Sn_2O_7$ samples synthesized at different solvothermal reaction times.

been observed as reaction time increased from 1 to 24 h. The absorption threshold of $Pr_2Sn_2O_7$ samples prepared for 1 h, 4 h and 8 h is located at about 294 nm, 320 nm and 325 nm, respectively, corresponding to a band gap of 3.8–4.2 eV, which is in good agreement with the reported value of SnO_2.[20-22] In the absorption spectrum, we can observe that the absorption edge of $Pr_2Sn_2O_7$ prepared for 12 h and 24 h is at around 296 nm (The band gap is about 4.19 eV), this absorption was assigned to the 4f–5d charge transitions of Pr^{3+} ion.[23] It is interesting to point out that there are other several strong absorption peaks in visible light. The strong absorption peaks appearing at around 443 nm (2.80 eV), 470 nm (2.64 eV), 483 nm (2.57 eV) and 582 nm (2.13 eV) are assigned to the 4f-4f transitions of Pr element.[23,24]

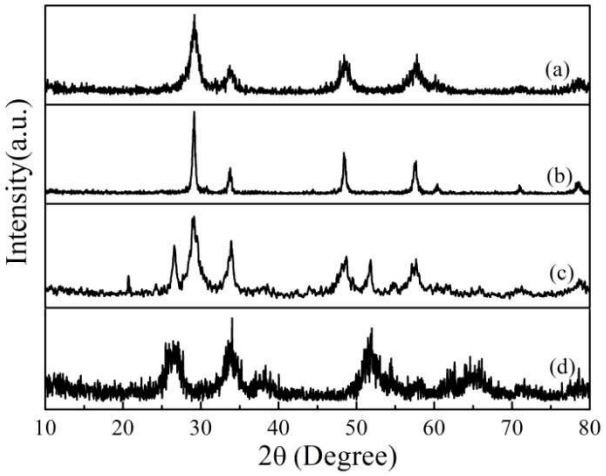

Fig.6 XRD patterns of the products obtained with different en/water volume ratios: (a) Ven/Vwater volume ratio of 14:1.(b) Ven/Vwater volume ratio of 2:1.(c)Ven/Vwater volume ratio of 1:2. (d) pure water as solvent.

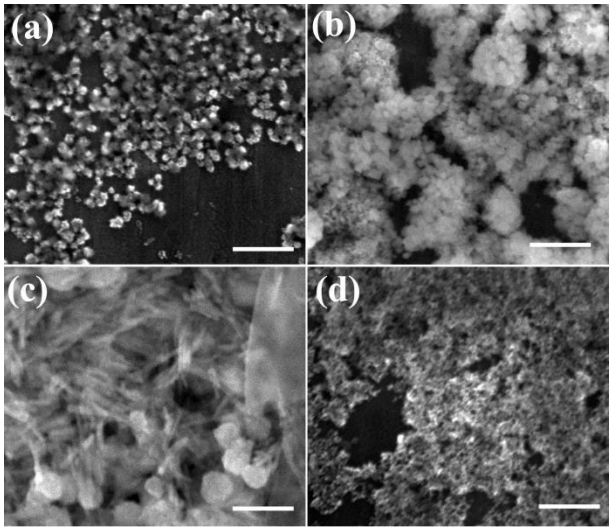

Fig. 7 FE-SEM images of the products obtained with different en/water volume ratios: (a) Ven/Vwater volume ratio of 14:1.(b)Ven/Vwater volume ratio of 2:1.(c)Ven/Vwater volume ratio of 1:2. (d) pure water as solvent. The scale bar is 200 nm.

To understand the formation mechanism of such $Pr_2Sn_2O_7$ nanospheres, different experimental conditions were investigated. The use of pure en as the solvent enables us to obtain the aforementioned $Pr_2Sn_2O_7$ nanospheres. Interestingly, when 15 mL en was replaced with 14 mL en and 1 mL water, while keeping the other reaction conditions the same, the product were still mainly composed of $Pr_2Sn_2O_7$ nanospheres with the size of about 10–30 nm as confirmed with XRD pattern and FE-SEM image (Fig.6a and Fig.7a). When the volume ratio en: H_2O reaches 2:1, the XRD peaks of prepared $Pr_2Sn_2O_7$ become narrower and the sample is mainly a mixture of granular aggregates with different sizes (Fig.6b and Fig.7b). By further increasing the volume of the water, there are some new diffraction peaks at ~26.6°, ~33.9 °, ~51.8 ° appeared, which can be attributed to the (110), (101) and (211) planes of tetragonal phase of SnO_2 (JCPDS, 41-1445), respectively. The sample is mainly a mixture of $Pr_2Sn_2O_7$ and SnO_2 particles with different morphologies (Fig.6c and Fig.7c). With pure water as the solvent, the XRD peaks ascribed to $Pr_2Sn_2O_7$ disappeared and all the peaks of the product could be readily indexed to tetragonal phase of SnO_2 (Fig.6d). The broadening of the diffraction peaks indicates the crystallite size of this SnO_2 sample is small, consistent with the observation of the FE-SEM image (Fig.7d). As a result, the solvent en plays key and complicated effects on generation of the $Pr_2Sn_2O_7$ nanospheres structure.

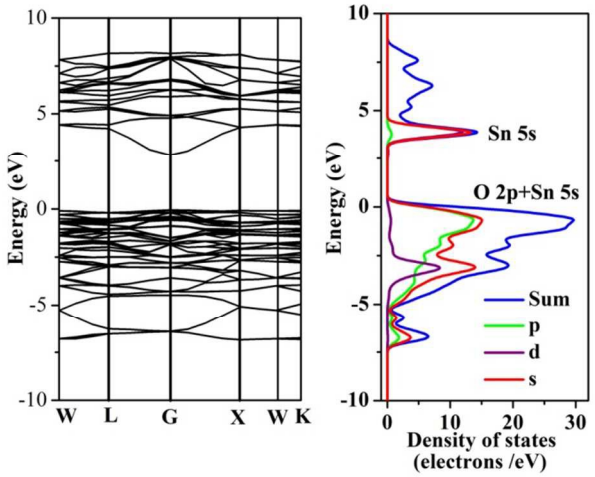

Fig.8 Energy-band diagram and density of states for $Pr_2Sn_2O_7$ calculated by a density functional method.

En is an excellent strong alkaline solvent which could act as reducing agent and coordinating agent in the formation of many micro/nanostructures.[1,25-27] It can adsorb on solid surfaces and control the velocity and direction of crystal growth. In the present case, the en molecules play multiple roles on the formation of $Pr_2Sn_2O_7$ nanospheres. At the beginning of the reaction, en molecules in the starting solution serve as the coordinating agent using a gauche conformation to chelate with Sn^{4+} and $Pr^{3+}$to form complex ions, such as $[Sn_m(en)_n]^{4+}$, $[Pr_x(en)_y]^{3+}$. During the solvothermal process, the complex ions were dissociated to from free Sn^{4+} ions and Pr^{3+} ions. There are little water form reactant $SnCl_4{\cdot}5H_2O$, Sn^{4+} ions are easily hydrolyzed to H_2SnO_3,which decomposes to amorphous SnO_2. Then amorphous SnO_2 reacts with free Pr^{3+} ions in the solution to form $Pr_2Sn_2O_7$

particles. At the same time, en molecules adsorb on solid surfaces during the reaction to form the $Pr_2Sn_2O_7$ nanospheres.

We also calculate the band structure of this material. Although the bandgap from Density Functional Theory (DFT) calculations is usually underestimated,[28-30] they nonetheless often provide important insight into the physicochemical behavior of the materials investigated. Fig.8 shows the energy-band dispersion and density of states of $Pr_2Sn_2O_7$ calculated using Cambridge Sequential Total Energy Package (CASTEP). From this figure we can see that $Pr_2Sn_2O_7$ is a direct-gap semiconductor material. It is important to note that the bottoms of the conduction bands are mainly composed of hybridized Sn 5s as well as a small quantity of O 2p orbitals. Whereas the tops of the valence bands are composed of hybridized O 2p and Sn 5s orbitals. A minimum band gap between VBM and CBM is about 2.80 eV, indicating of the presence of a semiconducting feature of the materials. The difference of band-gap value obtained by UV-vis spectrum (4.19 eV) and theoretical calculation (2.80 eV) was due to the underestimation by DFT calculation[28-30] and size quantization effect of nanomaterial.[31]

Although various properties of the pyrochlores have been investigated in recent years,[32-35] to the best of our knowledge, there are no published studies on the application of $Pr_2Sn_2O_7$. In this study, for the first time, we studied the gas-sensing performances of $Pr_2Sn_2O_7$ nanospheres and bulk $Pr_2Sn_2O_7$ to investigate the structural effects on their property. First, the thermal stability of the prepared samples was also evaluated by thermal gravimetric (TG) analysis. TG analysis shows no significant decomposition, and only 2.3% mass loss is observed up to 1000 °C (Fig.S3), which can be attributed to the desorption of en adsorbed on the surfaces of $Pr_2Sn_2O_7$ nanospheres. A long plateau is shown in the temperature range of 200–800 °C, indicating high thermal stability of the sample in air. Then bulk $Pr_2Sn_2O_7$ was obtained by conventional solid-state reaction (SSR) at 1200 °C for 16 h. Finally, the $Pr_2Sn_2O_7$ gas sensors were prepared. Fig. 9 summarizes the results of $Pr_2Sn_2O_7$ sensors. Fig.9(a) shows the dynamic gas response of the $Pr_2Sn_2O_7$ to various ethanol concentrations of 100, 200, 400 and 600 ppm at 300 °C. It can be clearly seen that $Pr_2Sn_2O_7$ nanospheres exhibit better responses to ethanol than SSR-$Pr_2Sn_2O_7$. Specifically, when $Pr_2Sn_2O_7$ nanospheres response to ethanol, the response and recovery times of the sensor to 100 ppm ethanol were less than 2 s and 22 s, respectively. As the ethanol concentration increased from 100 ppm to 600 ppm, the response of $Pr_2Sn_2O_7$ nanospheres and SSR-$Pr_2Sn_2O_7$ increased from 53.3 and 11.1 to 74.2 and 32.2, respectively. When exposed to 100 ppm ethanol, the responses are about 53.3 and 11.1 for $Pr_2Sn_2O_7$ nanospheres and SSR $Pr_2Sn_2O_7$ sample, respectively. In general, the response of semiconducting metal oxide gas sensors was dependent on the operating temperature due to the temperature-dependent gas adsorption and desorption on the oxide surface.[36-38] It can be seen from the Fig.9(b) that the ethanol response of $Pr_2Sn_2O_7$ nanospheres increased with the increasing of working temperature and then decreased as the temperature further increases. The $Pr_2Sn_2O_7$ nanospheres sensor revealed the maximum response at 300 °C. This agrees with the results from other ethanol gas sensors, showing that optimum operating temperatures ranged from 150 to 350 °C.[36,37]

The repeatability characteristic of $Pr_2Sn_2O_7$ nanospheres sensor was performed by exposing the sensor to ethanol gas concentration of 100 ppm for three exposure/recovery cycles (Fig.S4). The presented sensor shows an acceptable repeatability of ethanol gas sensing. It should be emphasized that the morphology of the $Pr_2Sn_2O_7$ nanospheres remained almost unchanged, except for a slight increase in size after 300 °C heat treatment for 2 h (Fig.S5), indicating the stability of the $Pr_2Sn_2O_7$ nanospheres under 300 °C heat treatment. Fig.9(c) shows the response of the $Pr_2Sn_2O_7$ nanospheres sensor towards various testing gases with the concentrations of 100 ppm at the operating temperature of 300 °C. Four kinds of gases have been tested, including C_2H_5OH, NH_3, CO and H_2. It is clear from Fig. 9(c) that the sensor exhibits the highest response towards C_2H_5OH , which suggests that selective detection of ethanol can be attained.

However the exact sensing mechanism of the $Pr_2Sn_2O_7$ nanospheres towards ethanol gas need to be further investigated.

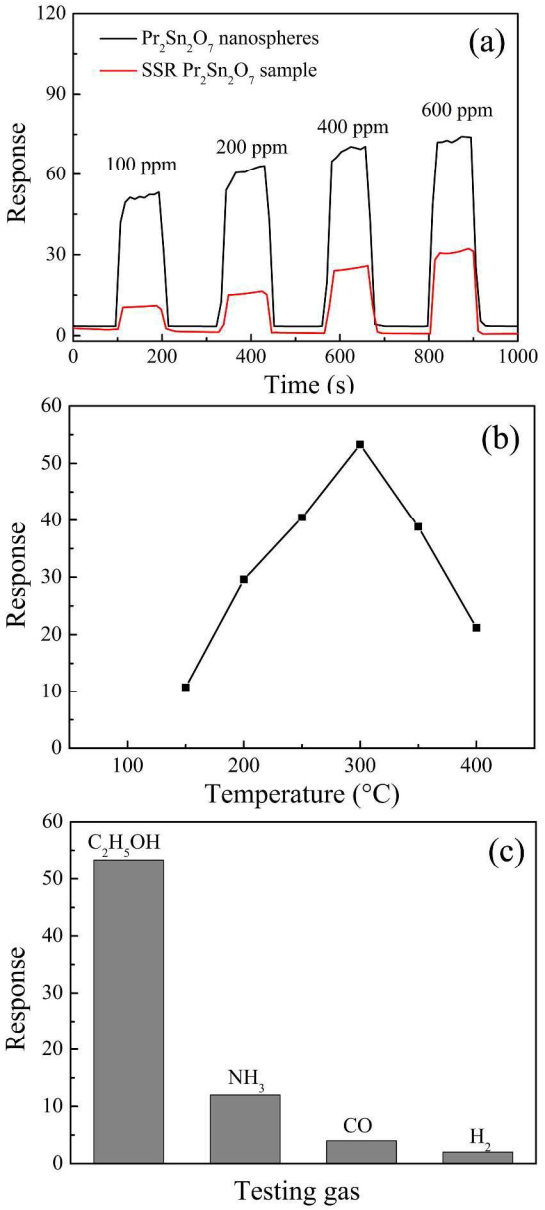

Fig.9 (a) Response of $Pr_2Sn_2O_7$ samples to ethanol of various concentrations at 300 °C; (b) Response of the $Pr_2Sn_2O_7$ nanospheres to 100 ppm ethanol at different operating temperatures.(c) Response of the $Pr_2Sn_2O_7$ nanospheres to various testing gases.

Most semiconducting oxide gas sensors are based on the conductivity changes caused by the adsorption and desorption of the gas molecules on the surface of the sensing structure.[39-41] When the sensing material is exposed to O_2 in the atmosphere, the interface of the sensing material adsorbs oxygen and produce oxygen ions with negative charge by capturing electrons from the conduction band. When the sensor is exposed to the ethanol at higher temperature, ethanol reacts with the adsorbed oxygen ions reducing their concentration and result in increasing the semiconductor conductivity. The enhancement of the ethanol gas sensing performance of $Pr_2Sn_2O_7$ nanospheres can be attributed to the wider band gap (size quantization effect of nanomaterial) and greater sensing surface area due to the nanosphere structure. Fig.10 shows nitrogen adsorption–desorption isotherms and pore size distribution curves (inset) of the $Pr_2Sn_2O_7$ nanospheres sample. The sample exhibits a type IV isotherm with an H3 hysteresis loop according to the Brunauer–Deming–Deming–Teller (BDDT) classification, indicating a meso-porous characteristic.[42,43] According to the Brunauer–Emmett–Teller (BET) and Langmuir methods, the specific surface areas of $Pr_2Sn_2O_7$ nanospheres are 89.2 and 124.4 m^2g^{-1}, respectively. The pore size distribution (inset in Fig.10) shows that $Pr_2Sn_2O_7$ nanospheres have the pore size distribution in the mesoporous region with a maximum peak pore diameter of 4.4 nm. These results are also consistent with SEM and TEM images results. After 300 ^oC heat treatment for 2 h, the BET and Langmuir surface areas of $Pr_2Sn_2O_7$ nanospheres are 72.5 and 100.6 m^2g^{-1}, respectively, which slightly decreased due to the crystal growth after heat treatment. The BET and Langmuir surface areas of the SSR-$Pr_2Sn_2O_7$ samples are 8.5 and 13.9 m^2/g, respectively, which explain the better gas-sensing performance of $Pr_2Sn_2O_7$ nanospheres than that of SSR-$Pr_2Sn_2O_7$ sample. Nitrogen adsorption–desorption isotherm liner plot of prepared samples are given in the supporting information (Table S1, Table S2 and Table S3).

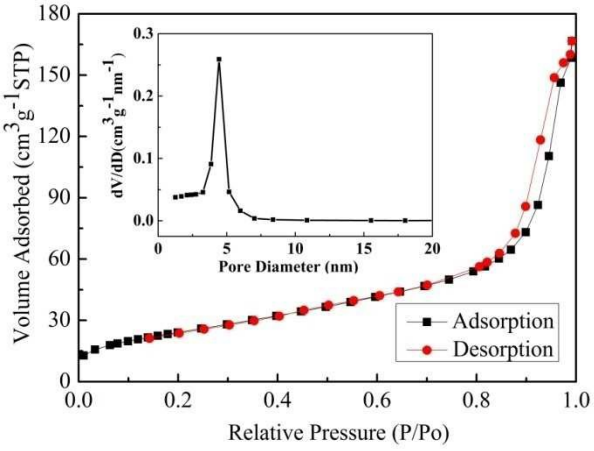

Fig.10 Nitrogen adsorption–desorption isotherms of the prepared $Pr_2Sn_2O_7$ nanospheres. Inset: the pore size distribution.

Conclusions

In summary, uniform $Pr_2Sn_2O_7$ nanospheres were successfully synthesized via a simple solvothermal route with ethylenediamine (en) as the solvent. The as-prepared $Pr_2Sn_2O_7$ nanospheres with the diameters 20–50 nm are composed of nanoparticles with average sizes of 3–5 nm. In our experiments, the solvent en has an important influence in the generation of $Pr_2Sn_2O_7$ nanospheres. The UV-vis spectrum reveals that the band-gap of synthesized $Pr_2Sn_2O_7$ nanospheres is about 4.19 eV, much higher than the theoretical calculation value by DFT (2.80 eV). For the first time, the gas-sensing performances of $Pr_2Sn_2O_7$ nanospheres was studied. Compared to SSR-$Pr_2Sn_2O_7$ sample, the enhanced gas sensing performances of $Pr_2Sn_2O_7$ nanospheres could be attributed to the unique mesoporous nanospheres, facilitating the gas diffusion and mass transportation in sensing materials. Moreover, it is anticipated that $Pr_2Sn_2O_7$ nanospheres could enable potential applications in photocatalytic reaction like some reported lanthanide stannate pyrochlores.

Acknowledgment

This work was supported by the National Natural Science Foundation of China (No. 51302001 and 21301002), Anhui Province College Excellent Young Talents Fund (No. 2013SQRL036ZD) and Funds for Distinguished Young Scientists of Anhui Polytechnic University (No. 2015JQ02).

Notes and references

1 Q. Liu, Y. Zhou, J. Kou, X. Chen, Z. Tian, J. Gao, S. Yan and Z. Zou, *J.Am. Chem. Soc.*, 2010, 132, 14385-14387.
2 H. Tong, S. Ouyang, Y. Bi, N. Umezawa, M. Oshikiri and J. Ye, *Adv. Mater.*, 2012, 24, 229-251.
3 X. W. Xie, Y. Li, Z. Q. Liu, M. Haruta and W. J. Shen, *Nature*, 2009, 458, 746-749.
4 Q. Liu, W. Zhang, R. Liu and G. Mao, *Eur. J. Inorg. Chem.*, 2015, 2015, 845-851.
5 H. G. Yang and H. C. Zeng, *J. Phys. Chem. B*, 2004, 108, 3492-3495.
6 J. Zhang, J. Liu, Q. Peng, X. Wang and Y. Li, *Chem. Mater.*, 2006, 18, 867-871.
7 S. Ding, J. S. Chen, G. Qi, X. Duan, Z. Wang, E. P. Giannelis, L. A. Archer and X. W. Lou, *J. Am. Chem. Soc.*, 2011, 133, 21-23.
8 J. Feng, B. Xiao, Z. X. Qu, R. Zhou and W. Pan, *Appl. Phys. Lett.*, 2011, 99, 201909.
9 K. E. Sickafus, L. Minervini, R. W. Grimes, J. A. Valdez, M. Ishimaru, F. Li, K. J. McClellan and T. Hartmann, *Science*, 2000, 289, 748-751.
10 M. Pirzada, R. W. Grimes, L. Minervini, J. F. Maguire and K. E. Sickafus, *Solid State Ionics*, 2001, 140, 201-208.
11 J. Feng, B. Xiao, R. Zhou and W. Pan, *Scr. Mater.*, 2013, 69, 401-404.
12 J. Lian, K. B. Helean, B. J. Kennedy, L. M. Wang, A. Navrotsky and R. C. Ewing, *J. Phys. Chem. B*, 2006, 110, 2343-2350.
13 A. J. Princep, D. Prabhakaran, A. T. Boothroyd and D. T. Adroja, *Phys. Rev. B*, 2013, 88, 104421.
14 A. P. Ramirez, A. Hayashi, R. J. Cava, R. Siddharthan and B. S. Shastry, *Nature*, 1999, 399, 333-335.
15 H. D. Zhou, C. R. Wiebe, J. A. Janik, L. Balicas, Y. J. Yo, Y. Qiu, J. R. D. Copley and J. S. Gardner, *Phys. Rev. Lett.*, 2008, 101, 227204.
16 S. Saha, S. Prusty, S. Singh, R. Suryanarayanan, A. Revcolevschi and A. K. Sood, *J. Solid State Chem.*, 2011, 184, 2204-2208.
17 Y. Mao, G. Li, W. Xu and S. Feng, *J. Mater. Chem.*, 2000, 10, 479-482.
18 J. Zeng, H. Wang, Y. Zhang, M. K. Zhu and H. Yan, *J. Phys. Chem. C*, 2007, 111, 11879-11887.
19 W. Wang, S. Liang, J. Bi, J. C. Yu, P. K. Wong and L. Wu, *Mater. Res. Bull.*, 2014, 56, 86-91.
20 W. Wu , S. Zhang , J. Zhou , X. Xiao , F. Ren and C. Jiang, *Chem. Eur. J.*, 2011, 17, 9708-9719.
21 Z. Li, Y. Zhou, T. Yu, J. Liu and Z. Zou, *Crystengcomm*, 2012, 14, 6462-6468.
22 Ç. Kılıç and A. Zunger, *Phys. Rev. Lett.*, 2002, 88, 095501.
23 K. Horchani-Naifer and M. Férid, *Inorg. Chim. Acta*, 2009, 362, 1793-1796.

24 H. Lv, X. Shen, Z. Ji, K. Chen and G. Zhu, *New J. Chem.*, 2014, 38, 2305-2311.
25 W.-T. Yao and S.-H. Yu, *Adv. Funct. Mater.*, 2008, 18, 3357-3366.
26 Y. Li, H. Liao, Y. Ding, Y. Fan, Y. Zhang and Y. Qian, *Inorg. Chem.*, 1999, 38, 1382-1387.
27 Z. Li, Y. Zhou, J. Song, T. Yu, J. Liu and Z. Zou, *J. Mater. Chem. A*, 2013, 1, 524-531.
28 S. Piskunov, E. Heifets, R. I. Eglitis and G. Borstel, *Computational Materials Science*, 2004, 29, 165-178.
29 C. Di Valentin, G. Pacchioni, A. Selloni, S. Livraghi and E. Giamello, *J. Phys. Chem. B*, 2005, 109, 11414-11419.
30 Z. Yi, J. Ye, N. Kikugawa, T. Kako, S. Ouyang, H. Stuart-Williams, H. Yang, J. Cao, W. Luo, Z. Li, Y. Liu and R. L. Withers, *Nat Mater*, 2010, 9, 559-564.
31 S. Baral, A. Fojtik, H. Weller and A. Henglein, *J. Am. Chem. Soc.*, 1986, 108, 375-378.
32 D. R. Modeshia and R. I. Walton, *Chem. Soc. Rev.*, 2010, 39, 4303-4325.
33 S. Ikeda, M. Fubuki, Y. K. Takahara and M. Matsumura, *Appl. Catal. A-Gen.*, 2006, 300, 186-190.
34 H. Y. Xiao, W. J. Weber, Y. Zhang, X. T. Zu and S. Li, *Sci.Rep.*, 2015, 5, 8265.
35 R. Perriot and B. P. Uberuaga, *J. Mater. Chem. A*, 2015, 3, 11554-11565.
36 H. N. Hieu, N. M. Vuong, H. Jung, D. M. Jang, D. Kim, H. Kim and S.-K. Hong, *J. Mater. Chem.*, 2012, 22, 1127-1134.
37 G. Sakai, N. Matsunaga, K. Shimanoe and N. Yamazoe, *Sensors and Actuators B: Chemical*, 2001, 80, 125-131.
38 A. P. Lee and B. J. Reedy, *Sensors and Actuators B: Chemical*, 1999, 60, 35-42.
39 C. D. Gu, H. Zheng, X. L. Wang and J. P. Tu, *RSC Adv.*, 2015, 5, 9143-9153.
40 D. Zhang, J. Liu, H. Chang, A. Liu and B. Xia, *RSC Adv.*, 2015, 5, 18666-18672.
41 H. Yan, P. Song, S. Zhang, Z. Yang and Q. Wang, *RSC Adv.*, 2015, 5, 79593-79599.
42 S. C. Yan, S. X. Ouyang, J. Gao, M. Yang, J. Y. Feng, X. X. Fan, L. J. Wan, Z. S. Li, J. H. Ye, Y. Zhou and Z. G. Zou, *Angew. Chem.*, 2010, 122, 6544-6548.
43 X. W. Lou, D. Deng, J. Y. Lee and L. A. Archer, *J. Mater. Chem.*, 2008, 18, 4397-4401.

Cite this: DOI: 10.1039/c0xx00000x

www.rsc.org/xxxxxx

ARTICLE TYPE

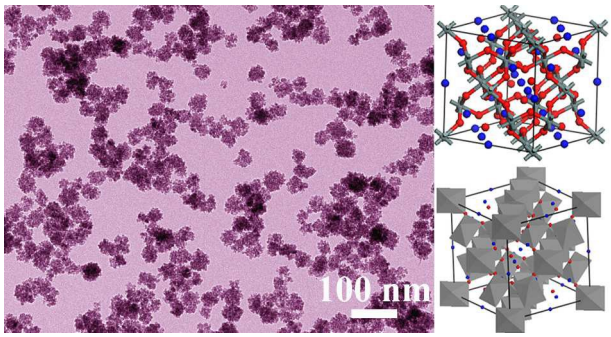

Uniform pyrochlore $Pr_2Sn_2O_7$ nanospheres with the diameters of 20–50 nm were synthesized through a simple solvothermal route with ethylenediamine as the solvent and the enhanced gas sensing performances of $Pr_2Sn_2O_7$ nanospheres could be attributed to the unique mesoporous nanospheres.